Field effect in manganite ultrathin films: Magnetotransport and localization mechanisms

I. Pallecchi, L. Pellegrino, E. Bellingeri, A. S. Siri, and D. Marré
CNR-INFM LAMIA, Corso Perrone 24, 16152 Genova, Italy

A. Tebano and G. Balestrino
CNR-INFM Coherentia and Department of Mechanical Engineering, University of Roma Tor Vergata, Roma, Italy
(Received 27 November 2007; revised manuscript received 14 May 2008; published 15 July 2008)

In this paper, we report on field-effect experiments in $La_{0.7}Sr_{0.3}MnO_3$ side-gate channels patterned on ultrathin epitaxial films having thickness ranging from 12 to 4 unit cells. Transport mechanisms and competition between phases, under the effect of electric and magnetic fields, as well as of other perturbations such as disorder and proximity to the interface with substrate are explored. We observe, in a 7 unit cells thick sample, a shift of the metal-insulator transition temperature as high as 43 K and a resistivity modulation up to 250% at low temperatures. In striking contrast, the 6–4 unit cells thick samples result to be insulating and almost insensitive to field-effect modulation. Such a finding indicates that for films thinner than 7 unit cells, a strong localization mechanism develops, which cannot be healed by band refilling. On the other hand, our results are compatible with a Mn e_g orbital rearrangement driven by the broken translational symmetry at the surface and/or interface, which suppresses the double-exchange mechanism and localizes the carriers.

DOI: 10.1103/PhysRevB.78.024411 PACS number(s): 75.47.Lx, 85.30.Tv, 75.70.Ak, 85.75.−d

I. INTRODUCTION

Manganites are widely studied materials in view of oxide electronics and spintronics applications, due to their highly spin-polarized current,[1] their colossal and low-field magnetoresistivities, and their Curie temperature above room temperature. Many devices and heterostructures have been realized, exploiting multiferroic properties,[2,3] lattice strain,[4,5] spin polarized tunneling,[6,7] spin polarized current injection,[8,9] resistive hysteretic switching,[10,11] phase separation,[12] carrier depletion at *pn* interfaces,[13–15] photocarrier injection,[16] and exchange interaction.[17]

Electric field effect on manganites has attracted much attention for its twofold potential: it can be used for probing the manganite phase diagram by carrier density modulation and for possible devices applications.

In fact a number of different field-effect devices have been realized, even integrated on silicon.[18] However, a variety of different and sometimes even contradictory behaviors have been reported: a shift of the metal-to-insulator transition temperature[19,33,20] up to 35 K,[21] a large (30%) resistivity modulation with no shift of the metal-to-insulator transition temperature at all,[22] an ambipolar gate effect[23] (that is enhanced conductance for both polarities of the gate voltage as opposed to the more common monotonic increase of conductance with decreasing gate voltage), an enhancement of the electric field effect in a magnetic field,[24,25] a complete suppression of the metallic state by ferroelectric field effect in ultrathin films,[26] a tuning of ferromagnetic response,[27] a competition between field effect and electrostriction as a function of film thickness,[28,29] and a dependence of anisotropic magnetoresistivity on carrier density.[30] Most of these studies are based on ferroelectric field effect, so as to avoid gate leakage currents. However, in the ferroelectric field effect, only two discrete states of polarization are possible, whereas in conventional field effect, the applied field can be varied continuously. Furthermore, it is clear that, because of the high hole concentration typical of these compounds (larger than 10^{21} cm^{-3}), the relative field induced change observed in the dc transport is hardly appreciable, except for ultrathin films, whose thickness is not much larger than electric-field penetration depth (nearly 0.2 nm in optimally doped films[26]).

Obviously, the issue of miniaturization, both in the film plane and along the film growth direction, is a relevant target for research purposes and for electronics applications as well. Thanks to recent improvements in nanopatterning techniques, systems having in-plane nanometer size have been realized in manganites by electron-beam lithography,[31] local anodization by atomic force microscopy,[32,33,12] and focused ion beam.[34] On the other hand, film thickness in manganites plays a crucial role in transport and magnetic properties,[35] because of the presence of a so-called "dead layer," at the film-substrate interface and/or at the film surface, few nanometres thick, with depressed magneto-transport properties. The study of this phenomenon may shed light on the origin of some unwanted drawbacks, related to lattice strain and interface and surface effects in manganites, such as spin depolarization at the surfaces and interfaces.[36,37] Indeed, the study of the magneto-transport properties in ultrathin manganite films belongs to the recently developing field of interfaces in oxide heterostructures: charge transfer and band bending at the interface between oxide compounds have been successfully realized[38–41] and modeled in the framework of a rigid-band description.[39,36] However, a satisfactory understanding of the origin and the properties of the "dead" layer in manganite films is still lacking, despite this, problem has been widely studied. First, it is still not clear if the dead layer lies at the film-substrate interface, at the film surface or else at both of them: in this respect, it must be noticed that manganite nanoparticles, too, exhibit a magnetic dead layer effect that increases as the particle size decreases.[42,43] A recent theoretical work has evidenced the role of lattice strain in triggering the electronic phase separation:[44] however, there is an almost universal agreement on the circumstance that lattice strain cannot be the sole responsible for the pres-

 ©2008 The American Physical Society

ence of the dead layer. Many authors[45–47] measured a dead layer thickness of 3–5 nm in $La_{0.7}Sr_{0.3}MnO_3$ and 6–15 nm in $La_{0.7}Ca_{0.3}MnO_3$ epitaxial films, estimated from the intercept of conductance versus film thickness linear plot. They found that the dead layer thickness depends on the nature of the substrate, but neither strain effects nor initial layers growth mode alone can account for it. It was suggested that chemically and/or structurally degraded microstructure at the interfaces may be responsible for it. Borges *et al.*[48] studied the different natures of magnetic and electric dead layers in manganite thin films. According to these authors, the latter is thinner and possibly related either to poor crystalline quality close to the interface and/or surface, or to narrowing of e_g bandwidth because of unpaired Mn–O bonds. On the other hand, the magnetic dead layer is a few nanometres thick and possibly related to the presence of weakly coupled not collinear spins that determine lower Curie temperature and lower coercivity, locally, in the sample. Ogale *et al.*[49] suggested that charge localization in the dead layer may be caused by a Jahn–Teller strain field induced by lattice mismatch, which lifts the degeneracy of the e_g levels. Such a strain field, if stronger than a critical value, may even trigger a phase transition to an antiferromagnetic insulating phase.[50] Recent linear dichroism of x–ray absorption spectroscopy (LD XAS) measurements indicated that in the dead layer, an orbital reconstruction freezes the conduction electrons inside the $e_g(3z^2\text{-}r^2)$ orbitals, thus suppressing the double-exchange mechanism.[51] The presence of 2–3 atomic layers of antiferromagnetic phase at the surface has been also theoretically predicted in Ref. 52 as a consequence of electronic orbital reconstruction at the surface. According to these authors, a shift of one or both the e_g orbitals at the surface may be effective in changing the relative population of $e_g(3z^2\text{-}r^2)$ and $e_g(x^2\text{-}y^2)$ orbitals. This suggests that, similarly, an electrostatic shift of the bands driven by field effect may tune the relative band population and restore ferromagnetic metallic state at the surface.

In this work, we plan to investigate how charge-carrier modulation and magnetic field tune the conductance of ultrathin $La_{0.7}Sr_{0.3}MnO_3$ epitaxial films. We analyze magnetotransport under field effect on a large number of $La_{0.7}Sr_{0.3}MnO_3$ epitaxial films of different thickness and degree of disorder. This study may help in understanding how external perturbations such as electric and magnetic fields, proximity to interface and/or surface and disorder do compete or cooperate in triggering localization mechanisms and phase separation in these strongly correlated systems. More specifically, we will try to clarify if the origin of the dead layer is related to a localizing mechanism, insensitive to the charge-carrier density, or rather to a charge depletion phenomenon, connected with rigid band bending at the interface, which could be compensated by an external injection of carriers.

II. EXPERIMENT

Ultrathin $La_{0.7}Sr_{0.3}MnO_3$ (thickness from 12 down to 4 unit cells, i.e., from 4.63 to 1.54 nm) film are deposited on (100)-$SrTiO_3$ substrates by pulsed laser ablation. A few unit cells thick $SrTiO_3$ buffer layer and a 15–75 unit cells thick cap layer are deposited below and over the manganite film. In Fig. 1, atomic control of the layer-by-layer growth process is demonstrated by *in situ* monitoring of RHEED (reflection high energy electron diffraction) oscillations. The presence of a $SrTiO_3$ cap layer suppresses the manganite-air interface, so that our samples have two identical manganite-$SrTiO_3$ interfaces. Additional details on the growth technique and structural characterization of films are given in Ref. 53.

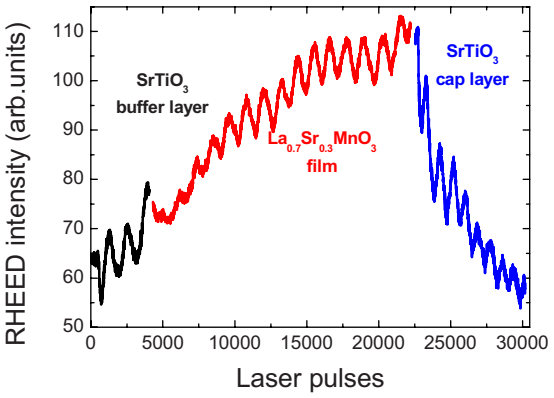

FIG. 1. (Color online) RHEED oscillations of layer-by-layer growth of a sample made of a 3 unit cells thick $SrTiO_3$ buffer layer, a 8 unit cells thick $La_{0.7}Sr_{0.3}MnO_3$ film and a protective 15 unit cells thick $SrTiO_3$ cap layer.

Films are then patterned by optical lithography and subsequently wet etched in HF10% solution to remove $SrTiO_3$ and in HCl vapors to remove $La_{0.7}Sr_{0.3}MnO_3$. This preparation procedure does not affect the transport properties of the film. Devices in side-gate geometry, with $w=5$ μm wide active channels and 15 μm wide gaps between the channel and the gate electrodes, are finally obtained. The computed capacitance[54] per unit length of the channel is nearly $4.5^*\varepsilon_r pF/m$, where ε_r is the temperature and electric-field dependent dielectric constant of the $SrTiO_3$ substrate. The capacitance is largely independent on film thickness t, as long as $t \ll w$, which means that the thinner the film, the larger the total accumulated or depleted charge per unit volume. We point out that in this geometry the electric field lines reach the channel from the gate electrodes, bending through the substrate and the air. As the relative $SrTiO_3$ dielectric constant is as large as 300 at room temperature and increases as T^{-1} with decreasing temperature,[55] the free-surface charge, proportional to the normal component of the displacement vector D, is mostly accumulated or depleted at the channel-substrate interface: hence, the importance of the role of the dead layer.

Assuming $\varepsilon_r \approx 300$ for $SrTiO_3$ at 300 K and $\varepsilon_r \approx 2000$ at 10 K and high electric field, it turns out that the total density of accumulated or depleted charge in a fully conductive 10 unit cells thick channel, is $4.3 \cdot 10^{18}$ and $2.9 \cdot 10^{19}$ cm^{-3} with with a 10 V gate voltage applied, at 300 and 10 K, respectively. This is an appreciable fraction of the carrier density in optimally doped manganites. In terms of charge per unit area, this means $1.6 \cdot 10^{12}$ and $1.1 \cdot 10^{13}$ cm^{-2} at 300 and 10 K, respectively, which is only one order of magnitude smaller than the best value obtained using ferroelectric

stacked layers geometries.[56,21] On the other hand, the side-gate geometry allows to circumvent problems related to electrical shorts caused by pinholes and defects across the insulating layer. Moreover, it relies on the optimal crystalline quality of the single-crystal substrate, which guarantees the largest possible dielectric constant and breakdown electric-field values compatible with the chosen material, that is $SrTiO_3$ in our case. In dielectric thin films, instead, both these quantities are significantly depressed.

As a further check, we have compared field-effect experimental results obtained in side-gate and back gate geometries. In the latter case, the gate voltage is applied to the back of the 0.5 mm thick $SrTiO_3$ substrate and the corresponding capacitance per unit length is $0.088^{*}\varepsilon_r pF/m$, 50 times smaller than for the side-gate geometry. The calculated capacitances are indeed consistent with our field-effect data.

Measurements of magnetotransport properties are carried out at temperatures from 10 K up to room temperature and in magnetic fields perpendicular to the film plane up to $\mu_0 H = 9$ T.

Some measurements do not reach room temperature because in the sample chamber of our apparatus the insulation above the water melting freezing point 273 K is poor due to the presence of humidity, so that the gate voltage cannot be safely applied, because it results in leakage currents and electrochemical reactions in the samples. Furthermore, above room temperature, migration of oxygen vacancies in the $SrTiO_3$ substrate causes gate leakage as well.

The maximum applicable gate voltage before reaching the leakage onset, even though not exactly the same for all samples, stays in the range of several tens of volts, corresponding to electric fields close to the $SrTiO_3$ breakdown value. Such differences in the breakdown gate voltages are likely due to the residual presence of tips, protrusions or roughness at the electrodes, remained after the lithographic and etching processes. The similarities among the different resistivity versus gate voltage curves supports the hypothesis that the maximum applied electric field is the same for all samples, despite the small differences in the gate voltages.

III. RESULTS AND DISCUSSION

A. Magnetotransport and field effect

Transport measurements show systematically that 7 unit cells thick or thicker samples exhibit metallic behavior below a characteristic metal-insulator transition temperature T_{MI}, whereas thinner samples are insulating in the whole temperature range.

In Fig. 2, left-hand panels, we show resistivity measurements as a function of gate voltage for different out-of-plane magnetic fields and temperatures for a 12 unit cells thick sample (sample A), with metal-insulator transition temperature $T_{MI} \approx 216$ K. The resistivities for all samples investigated in this paper must be considered as average values, as they are obtained from resistance values disregarding the circumstance that 6 unit cells are dead, which is much less conducting than the other ones. In the right-hand panels, the curves are plotted as relative variations from their zero gate voltage value, in order to highlight the field effect at different

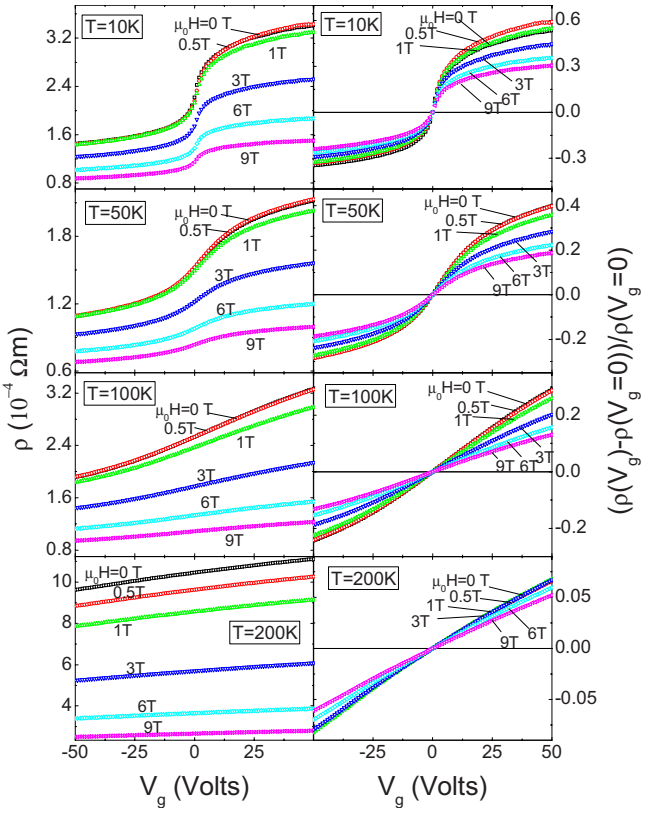

FIG. 2. (Color online) Left-hand panels: resistivity versus gate voltage curves of a 12 unit cells thick sample (sample A) at different magnetic fields and temperatures. Right-hand panels: relative resistivity change.

magnetic fields, independently of the negative magnetoresistivity (MR). The largest effect is observed at low temperature, that is at $T=10$ K in the uppermost panels, and it is -30% in the accumulation state ($V_g<0$) and $+60\%$ in the depletion state ($V_g>0$) at $\mu_0 H=0$. This is easily understood because in the depletion regime the carrier concentration decreases: as a consequence the electric-field penetration depth increases and the fraction of the depleted carriers to the total number of carriers is larger. At higher temperatures, the asymmetry with respect to the sign of the gate voltage decreases and, as T_{MI} is approached, the asymmetry is even reversed: in the lowest panel, at $T=200$ K the relative resistivity modulation are -6.7% and $+6.0\%$ in the accumulation and depletion states, respectively. This behavior is commonly found in all our metallic films and suggests that phase separation and percolative transport through metallic regions play a major role in a range of temperatures around the transition temperature. In a homogeneous system, the depletion resistivity change is expected to be either larger or nearly equal to the accumulation resistivity change in semiconducting and metallic samples, respectively. In addition, just below the transition temperature, a positive voltage that should drive the system even closer to the transition point, where fluctuations are enhanced, should have a more dramatic effect than a negative gate voltage. Instead, the opposite trend is observed, indicating that the key point is the intrinsic electronic inhomogeneity of the system. In the phase separated

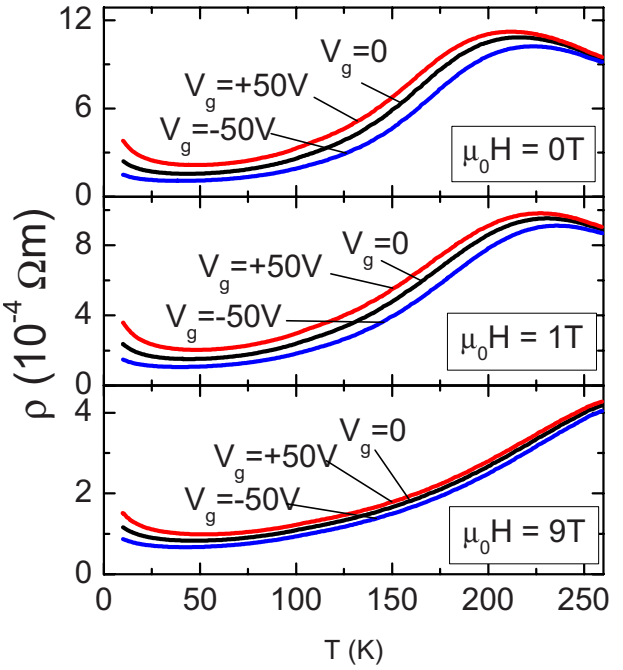

FIG. 3. (Color online) Resistivity versus temperature curves of the 12 unit cells thick sample A at different magnetic fields and gate voltages. The total T_{MI} shifts are 12 K and 9 K at $\mu_0 H=0$ and $\mu_0 H=1$ T, respectively.

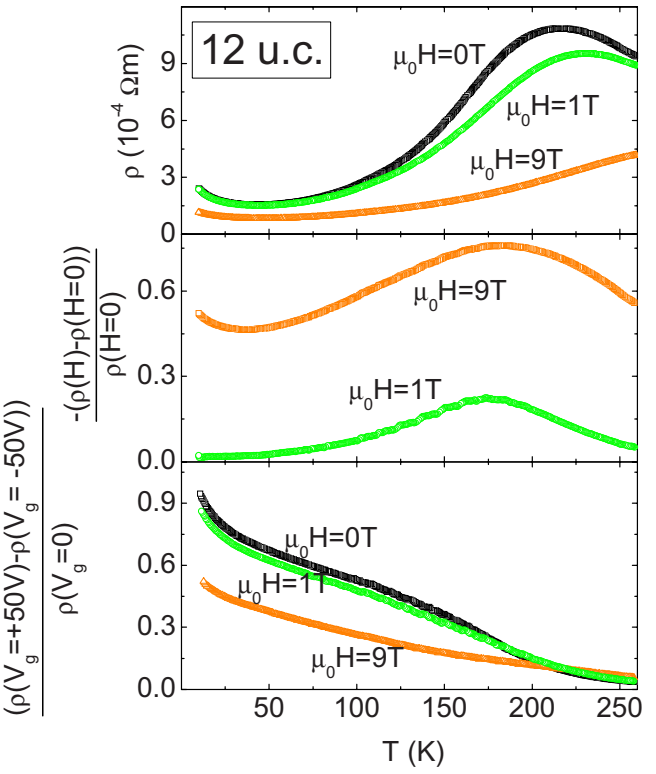

FIG. 4. (Color online) Top panel: resistivity versus temperature curves of the 12 unit cells thick sample A at different magnetic fields. Middle panel: absolute value of negative magnetoresistivity as a function of temperature at different magnetic fields. Bottom panel: relative resistivity modulation by field effect as a function of temperature at different magnetic fields.

regime, a negative voltage seems to be particularly effective in increasing the conductivity of semiconducting regions, where the electric field penetrates more deeply, or in shrinking the volume of such regions, thus resulting in a larger modulation of the resistivity along the percolative path. On the contrary, a positive gate voltage has lower efficiency in decreasing the conductivity and/or shrinking the volume of metallic regions. Another apparent effect in Fig. 2 is that at low temperature the resistivity curves exhibit nonlinear behavior, whereas they become increasingly linear with increasing temperature. This is certainly related to the nonlinear behavior of the dielectric constant ε_r of $SrTiO_3$: the low-temperature resistivity versus gate voltage curves (uppermost panel of Fig. 2) just replicate the shape of ε_r versus electric-field curve, which tends to saturate at high electric fields.[55] Furthermore, the relative resistivity modulation decreases with increasing temperature, which reflects the temperature behavior of the $SrTiO_3$ dielectric constant. However, it does not follow the T^{-1} dependence of the dielectric constant strictly because different transport and localization mechanisms come into play in the different temperature ranges, thus influencing in different ways the efficiency of field effect. Finally, it can be observed that in the whole temperature range, the relative resistivity modulation is larger in zero magnetic field and decreases monotonically with increasing H. This is as well a general feature found in all metallic samples and it is explained in terms of the increased metallic character of manganites in an applied magnetic field.[57,58]

In Fig. 3, we present resistivity versus temperature curves measured on the same 12 unit cells thick sample A for different magnetic fields and gate voltages $V_g=0$ and ± 50 V. In the uppermost panel, the T_{MI} in zero field is shifted 7 K upward by a negative gate voltage and 5 K downward by a positive one, with an overall shift of 12 K. We notice that the shift is asymmetric with respect to the gate voltage sign, in a way similar to the resistivity modulation in the phase-separation region around T_{MI}. Such a behavior indicates that the temperature dependence of the dielectric constant is not crucial, either because the temperature shift is not very large, or because it does not occur at the lowest temperatures where the temperature dependence of the dielectric constant is steepest, or else because at the high values of the electric fields used in the measurements (always larger than 10 MV/m), the variation of the dielectric constant with temperature is weak.[55] In a field of $\mu_0 H=1$ T, the $T_{MI} \approx 230$ K is shifted by 9 K. Again, similarly to the resistivity modulation, the transition temperature shift is always a monotonically decreasing function of the magnetic field, although its value is not universal, as it critically depends on sample thickness, strain, stoichiometry, and localization mechanisms. This is due to the combined effects of the increased metallic character of manganites in an applied magnetic field[57,58] and of the decrease of $SrTiO_3$ dielectric constant with increasing temperature.[55]

In Fig. 4, we summarize the effects of the electric and magnetic fields, as well as of the combination of the two, in sample A. It is tempting to distinguish the effects of the electric and magnetic fields by assuming that the former tunes the conductivity and the relative volume fractions of

metallic and semiconducting regions, whereas the latter, beside tuning the relative volume fractions of metallic and semiconducting regions, aligns the magnetic moments. However, the role of electric field in the double-exchange mechanism is not sharply distinguished from that of the magnetic field. The electric field increases the number of carriers, enhances the carrier mediated coupling between adjacent magnetic moments, and consequently contributes in aligning them. In turn, the magnetic field aligns Mn moments, enhances the transfer integral of the charge carriers, and consequently increases the conductivity similarly to the electric-field effect. In the top panel of Fig. 4, the resistivity curves at different magnetic fields are shown: the standard negative colossal MR and T_{MI} shift can be noticed. The weak resistivity upturn at low temperatures is probably related with localization induced by either disorder or additional strain caused by a slightly altered stoichiometry. The absolute value of the negative MR as a function of temperature is plotted in the middle panel of Fig. 4 for $\mu_0 H=1$ T and $\mu_0 H=9$ T. The characteristic broad peak reaches 76% at $\mu_0 H=9$ T and 22% at $\mu_0 H=1$ T and extends in a very broad range of temperatures below the transition, indicating a significant phase separation in these ultrathin films. In the bottom panel, the relative field-effect modulation $[\rho(V_g=+50\ \mathrm{V})-\rho(V_g=-50\ \mathrm{V})]/\rho(V_g=0)$ is plotted as a function of temperature at different magnetic fields. It can be seen that there is a similar broad peak extending in a wide range below the transition, which we consider a signature of the phase-separation regime. In addition, there is a superimposed monotonic increase with decreasing temperature, which eventually becomes steeper at the lowest temperatures. We attribute this increase again to the temperature behavior of the $SrTiO_3$ dielectric constant and the steeper slope below 25 K to the carrier localization, which decreases the total number of free carriers and enhances the relative field effect. By applying a magnetic field as large as 9 T, the broad peak disappears and turns into a featureless monotonic curve. Indeed, such a large magnetic field partially suppresses the phase-separation regime and aligns single spins and/or entire domains, thus lowering the overall field effect.

We now consider a thinner sample, namely sample B which is 10 unit cells thick and has a $T_{MI}\approx 210$ K. In Fig. 5, we show resistivity curves for different gate voltages and magnetic fields as a function of temperature. Similarly to the case of sample A, the effect is larger in depletion than in accumulation at low temperatures and the other way around above 150 K, in the phase separated regime. Magnetic field application results in an increased metallicity and a weaker field effect. The resistivity versus V_g curves (not shown) are nonlinear at low temperature due to the nonlinear dielectric constant of the substrate and become linear with increasing temperature. The field-effect modulation at low temperatures reaches −32% in the accumulation state and +97% in the depletion state at $T=10$ K, indicating that the screening length is a significant fraction of the film thickness. On the whole, the differences between samples A and B are merely quantitative, due to the different thickness and thereby to the different total number of charge carriers in the sample. In Fig. 5, the shift of the $T_{MI}\approx 210$ K in zero field is 8 K upward in the accumulation state and 6 K downward in the

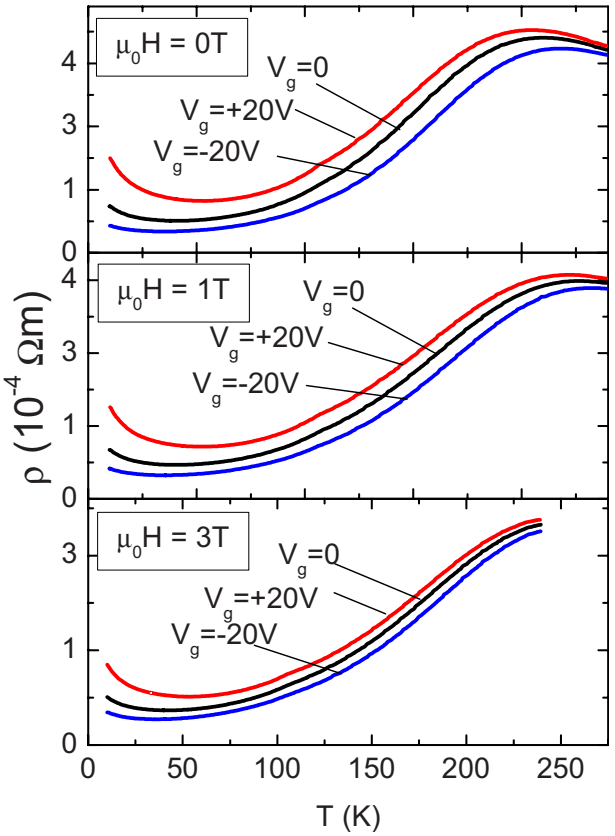

FIG. 5. (Color online) Resistivity versus temperature curves of a 10 unit cells thick sample (sample B) at different magnetic fields and gate voltages. The total T_{MI} shifts are 14 K and 11 K at $\mu_0 H=0$ and $\mu_0 H=1$ T, respectively.

depletion state, with an overall shift of 14 K. To summarize the results on sample B, in Fig. 6, we plot the resistivity curves at different magnetic fields (top panel), the absolute value of MR (middle panel) and the field-effect resistivity modulation $(\rho(V_g=+20\ \mathrm{V})-\rho(V_g=-20\ \mathrm{V}))/\rho(V_g=0)$ at different fields (bottom panel). Again, the qualitative considerations done for sample A still hold, but the field effect is larger.

We discuss now measurements on a 7 unit cells thick sample (sample C), which is the thinnest sample that still exhibits metallic conductivity with a $T_{MI}\approx 174$ K, even if, close to room temperature, its average resistivity is nearly 3–4 times larger than that of the metallic samples A and B. In Fig. 7, the resistivity versus temperature curves are shown for different gate voltages and magnetic fields. It can be seen that the sample is metallic only between ~70 K and T_{MI}, as its resistivity curve exhibits an evident low-temperature upturn. The T_{MI} is shifted by as much as 43 K in zero magnetic field (−18 K in the depletion state and +25 K in the accumulation state) and by 21 K at $\mu_0 H=9$ T. Despite the resistive transitions are quite large, such a shift is the largest ever obtained by standard (nonferroelectric) field effect, to the best of our knowledge. In Fig. 8, we notice that the MR presents a broad maximum which does not vanish far away from the transition temperature (middle panel), indicating an extended regime of phase separation. In the bottom panel, it can be seen that the field-effect modulation $(\rho(V_g=+30\ \mathrm{V})$

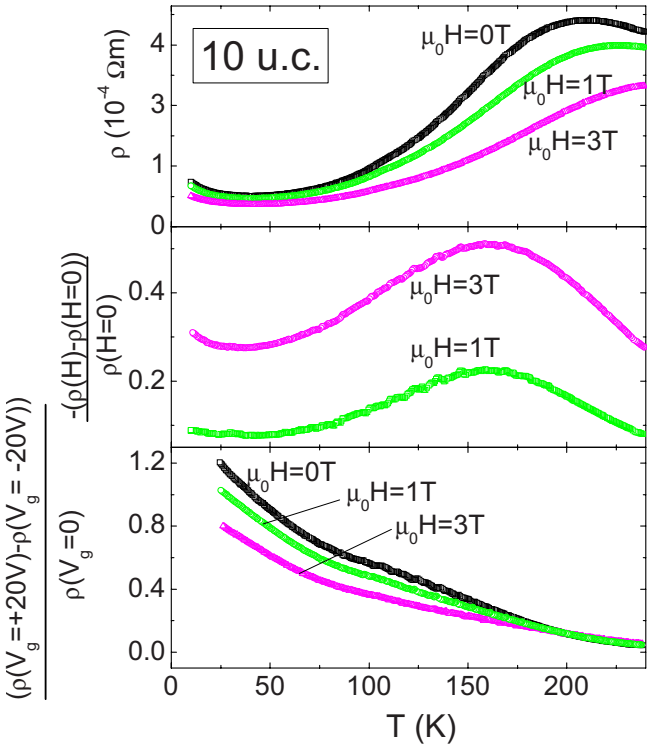

FIG. 6. (Color online) Top panel: resistivity versus temperature curves of the 10 unit cells thick sample B at different magnetic fields. Middle panel: absolute value of negative magnetoresistivity as a function of temperature at different magnetic fields. Bottom panel: relative resistivity modulation by field effect as a function of temperature at different magnetic fields.

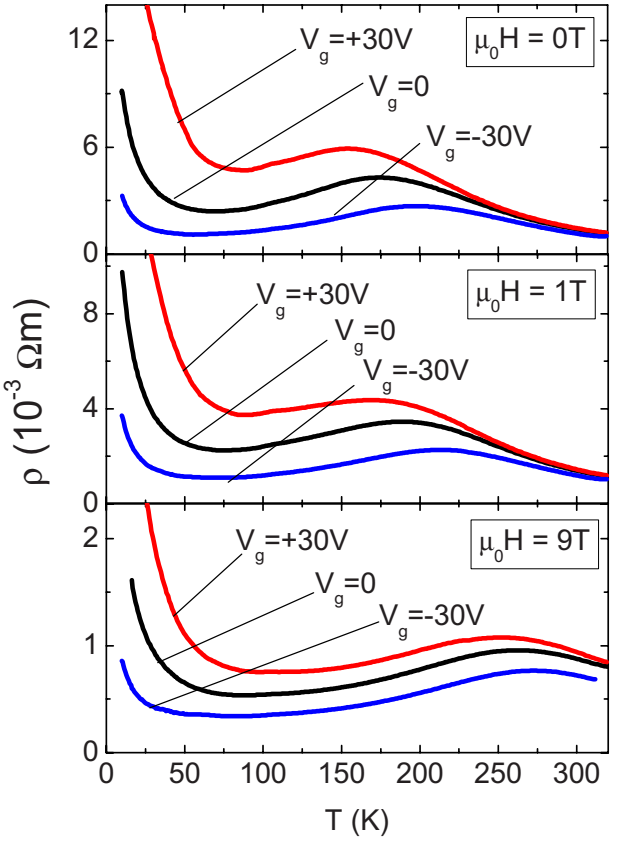

FIG. 7. (Color online) Resistivity versus temperature curves of a 7 unit cells thick sample (sample C) at different magnetic fields and gate voltages. The total T_{MI} shifts are 43 K at $\mu_0 H=0$ and $\mu_0 H=1$ T and 21 K at $\mu_0 H=9$ T.

$-\rho(V_g=-30\ \mathrm{V}))/\rho(V_g=0)$ reaches values as large as 250% at low temperature. Furthermore, the broad bumplike feature, which we relate to phase separation, is visible also in the field-effect curves.

B. Magnetotransport and field effect in the dead layer

We conclude our analysis with a 6 unit cells thick film (sample D). All samples with thickness of 6 unit cells or smaller do not exhibit metallic behavior at any temperature and have high resistivity. The field-effect experiments on sample D are feasible only above 175 K, due to the too high resistance of the patterned sample. In Fig. 9, the resistivity curves as a function of the gate voltage and at different magnetic fields show that a gate voltage of ± 50 V is able to yield a resistivity modulation of only $\sim 8\%$ at 175 K, with very weak dependence on the magnetic field. The weak dependence of field effect on magnetic field is a common feature observed in weakly localized samples. We notice that at the same temperature the 7 unit-cell sample C exhibits a resistance modulation of 75%, with an even smaller gate voltage ± 30 V, suggesting that a dramatic change in transport mechanisms occurs when the film thickness is reduced by a single unit cell, from 7 unit cells to 6 unit cells. This results is quite unexpected, because it is well known that field-effect resistivity modulation is enhanced in thinner films. Furthermore, if the insulating behavior of the 6 unit cells sample were to ascribe to a stronger carriers depletion phenomenon at the interface, relative to the metallic 7 unit cells sample, a larger field effect would be expected in the former sample, as a consequence of the deeper penetration of the electric field. In the uppermost panel of Fig. 10, the resistivity versus temperature curves of sample D for different magnetic fields are shown. There is no indication of an incipient transition to a metallic state, even at 9 T. The absolute value of negative MR, shown in the second panel of Fig. 10, turns out to be featureless and increases with decreasing temperature: it is very small at 1 Tesla, namely less than 10% as compared to values always larger than 20% in thicker samples. The absence of a metal-insulator transition and the small MR indicate that the double-exchange mechanism is depressed, even if not completely suppressed, in the dead layer. The resistivity curves for different gate voltages in zero magnetic field can be hardly distinguished form each other (third panel of Fig. 10). Again, no indication of a transition is detected, even in the accumulation regime. In the bottom panel, the field-effect resistivity modulation $[\rho(V_g=+50\ \mathrm{V})-\rho(V_g=-50\ \mathrm{V})]/\rho(V_g=0)$ is shown as a function of temperature. The field-effect modulation curves for different magnetic fields almost overlap, they are only weakly increasing with decreasing temperature and featureless.

In even thinner samples, down to 4 unit cells thickness, the overall behavior is very similar to that observed in

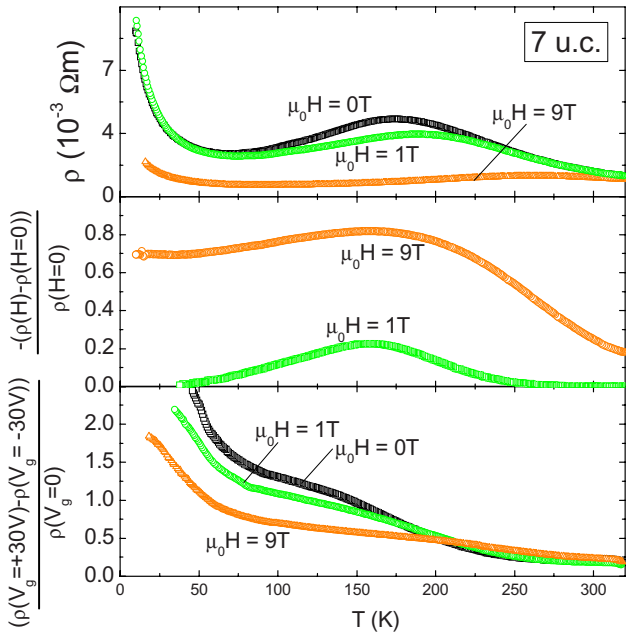

FIG. 8. (Color online) Top panel: resistivity versus temperature curves of the 7 unit cells thick sample C at different magnetic fields. Middle panel: relative resistivity modulation by field effect as a function of temperature at different magnetic fields. Bottom panel: absolute value of negative magnetoresistivity as a function of temperature at different magnetic fields.

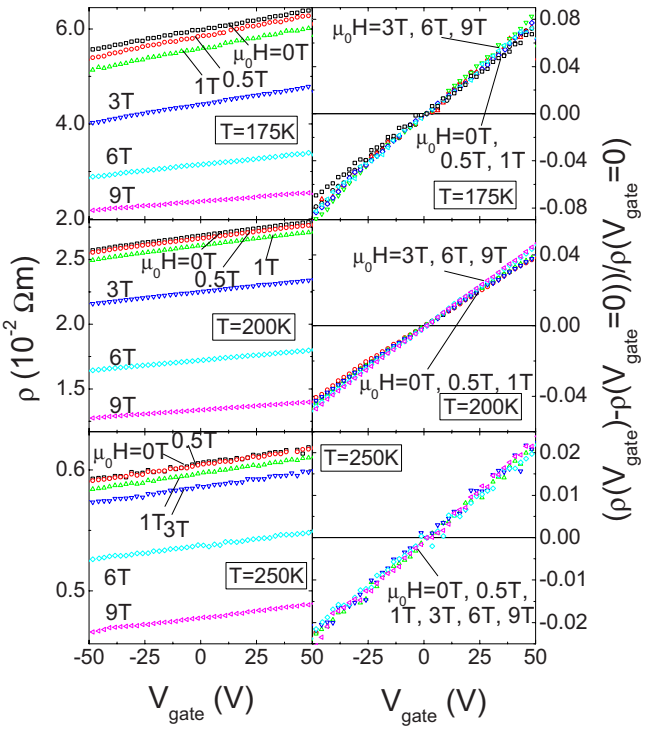

FIG. 9. (Color online) Left-hand panel: resistivity versus gate voltage curves of a 6 unit cells thick sample (sample D) at different magnetic fields and 175 K. Right-hand panel: relative resistivity change.

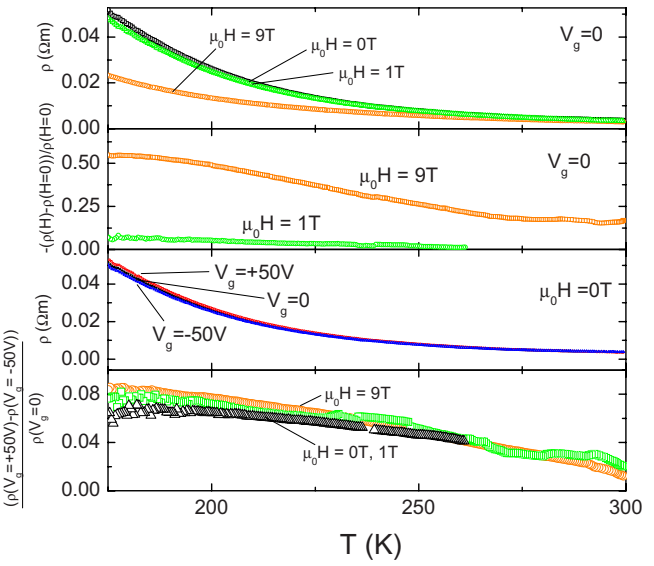

FIG. 10. (Color online) Top panel: resistivity versus temperature curves of the 6 unit cells thick sample D at different magnetic fields. Second panel: absolute value of negative magnetoresistivity as a function of temperature at different magnetic fields. Third panel: resistivity versus temperature curves in zero magnetic fields and at different gate voltages. Bottom panel: relative resistivity modulation by field effect as a function of temperature at different magnetic fields.

sample D, apart from the absolute value of MR that becomes smaller and smaller in thinner films, being at most 4% at 1 T in the 4 unit cells samples.

In Fig. 11, we report the carriers concentration in the 7 and 6 unit cells samples C and D, as deduced from the ordinary component of the Hall voltage V_H, i.e., in the linear V_H versus H regime at high magnetic field. As the temperature is lowered, the carrier density of the 7 unit cell sample decreases very weakly down to 50 K and faster below, in correspondence with the resistivity upturn. The carrier density in the 6 unit cell sample decreases faster than that of the 7 unit cell sample. Unfortunately, for sample C exhibiting metal-insulator transition at 174 K, only data points below

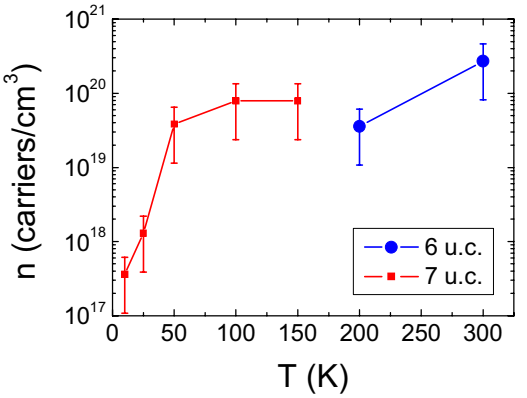

FIG. 11. (Color online) Carrier concentration as a function of temperature measured in the 7 and 6 unit cells samples, extracted from the normal contribution to the Hall effect. The lines are guides to the eye.

the transition are available, due to the presence of the anomalous component in the Hall-effect voltage close to the transition.[59] For sample D, only data above 200 K are available, as only in this temperature range the resistance is small enough to be measurable. Despite there is no overlap in these two temperature ranges, it is clear that the carrier concentrations in the two samples are not too much different. It is even likely that, at the same temperature, the carrier concentration of the 6 unit cell sample is smaller. In these conditions, field effect in the 6 unit cell sample should be larger rather than smaller. Together with insensitivity to field effect and temperature activated transport, these observations provide further unambiguous evidence that the localization mechanism active in the dead layer cannot be described in terms of charge depletion from rigid bands model, but rather in terms of a mechanism where the proximity of the interface plays a crucial role. Also the epitaxial strain can be ruled out as a cause for the dramatic change in the magnetotransport properties observed when reducing the film thickness from 7 to 6 unit cells, because all films in the investigated thickness range are fully strained.[60] We suggest that the double-exchange transport mechanism may be hindered—even if not completely destroyed—as a result of the rearrangement of band structure close to the interface with a consequent redistribution of charge carriers in localized states, not involved in the double-exchange transport. This conclusion is in agreement with the scenarios proposed on the basis of other experimental methods.[45,48,51] In particular, Tebano *et al.*[51] have recently shown, by LD XAS, that orbital reorganization, which occurs in ultrathin $La_{0.7}Sr_{0.3}MnO_3$ films on $SrTiO_3$ substrates as a consequence of the broken symmetry at the interface, stabilizes the $e_g(3z^2\text{-}r^2)$ against the $e_g(x^2\text{-}y^2)$ orbitals. This modification of the density of states involves few atomic layers. Preferential occupation of $e_g(3z^2\text{-}r^2)$ orbitals contributes to carriers localization suppressing the double-exchange ferromagnetic and metallic phase and enhancing the C antiferromagnetic and insulating phase where spins are coupled antiferromagnetically in the *ab* plane and ferromagnetically along the *c* axis. In this framework, the accumulation of carriers, which preferentially occupy the $e_g(3z^2\text{-}r^2)$ orbitals, by field effect, would not restore the double-exchange conduction mechanism. The present experiment shows that e_g bands redistribution at the surface due to broken symmetry is robust and cannot be restored by electrostatic shift of the bands by field effect.

Alternatively, it can be argued that charge reconstruction may be the cause for the insulating behavior of the six dead layers in manganites. Similarly to what occurs in perovskite oxide superlattices,[40,41] the growth of the polar $La_{0.7}Sr_{0.3}MnO_3$ on nonpolar $SrTiO_3$ may in principle cause a buildup of electric potential across the polar manganite film. In this scenario, as the electric potential overcomes a critical value, a polar catastrophe drives an electronic reconstruction at the film-substrate interface: namely, if it is assumed that the $La_{0.7}Sr_{0.3}O$ and MnO_2 layers have a +0.7 and −0.7 charges per unit cell, respectively, one could expect that, due to reconstruction, the very first layer adjacent to the substrate remains with +0.35 or −0.35 charges per unit cell, depending on the substrate termination, thus becoming severely insulating. However, this description implies that films of thickness

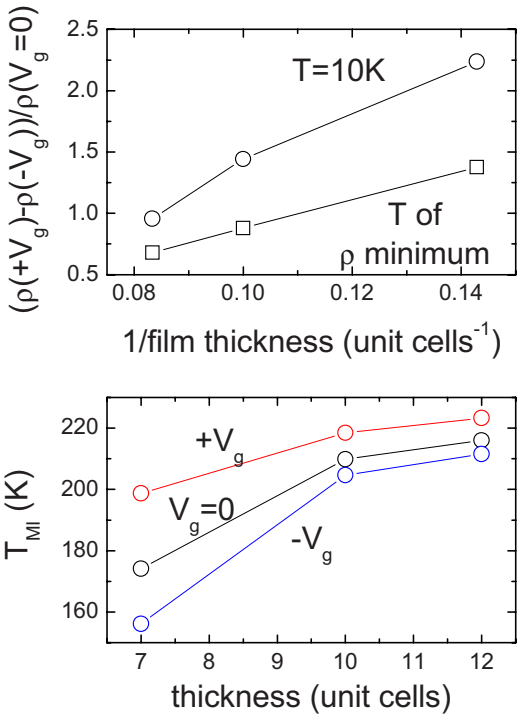

FIG. 12. (Color online) Top panel: field-effect relative resistivity modulation plotted as a function of the inverse film thickness for the metallic samples A, B, and C. Bottom panel: T_{MI} in the depletion (positive V_g), accumulation (negative V_g) and unperturbed states as a function of film thickness for the metallic samples A, B, and C.

smaller than the catastrophic value should not undergo electronic reconstruction and thereby should exhibit bulklike transport and a reentrant behavior of conductivity as a function of film thickness should be observed: assuming for example a critical thickness of 6 unit cells, the 2–4 unit cells films should be well conducting, similarly to the thick films, while the 6 unit cells films should be localized. On the contrary, we observe severe localization for all thickness values below 6 unit cells. Furthermore, the possibility of buildup of electric potential, relevant to ionic insulators, is questionable in a compound with such a large carrier density. In addition to these arguments, another reason for rejecting the explanation in terms of electronic reconstruction mechanism is that the dead layer in manganites is universally observed in all films, regardless they are grown on polar or nonpolar substrates and, however, small is the lattice mismatch.

We try now to get some information on the average charge concentration in the dead layer and in the adjacent few metallic layers, independently from Hall-effect data, by qualitative simple arguments. We consider the metallic samples A, B, and C, where there seem to be no evident additional effects of localization other than those that are inevitably present in ultrathin manganites, related to strain. In Fig. 12, upper panel, the relative change of resistivity due to field effect, defined as $\Delta\rho/\rho=[\rho(+V_g)-\rho(-V_g)]/\rho(V_g=0)$, is plotted as a function of the inverse film thickness, disregarding the fact that the maximum gate voltage applied is slightly different in each sample. Only sets of data at $T=10$ K and at the minimum of the resistivity versus tempera-

ture curves have been considered. Indeed, at higher temperatures, it is not evident how to compare resistivity changes of different samples, because any fixed temperature falls in a different regime of the sample transport behavior and, on the other hand, if we chose a certain characteristic point of the resistivity curve, say T_{MI}, the dielectric constant of the substrate is not the same at the different T_{MI} values of each sample. The latter problem is negligible, if we chose the minima of the resistivity curves, as they fall at $T \approx 47$ K, $T \approx 52$ K, and $T \approx 88$ K in samples A, B, and C, respectively, and it is known that the dielectric constant of $SrTiO_3$ changes little below $T \approx 100$ K in high electric fields (we assume here $\varepsilon_r \approx 2000$).[55] The former problem can be tentatively neglected as well at $T=10$ K, because all the samples are in the regime of the resistivity upturn. To a first approximation, disregarding the complex scenario of phase separation and considering average effective values of charge density and resistivity, we expect the following relationship for the data points in the upper panel of Fig. 12:

$$\frac{\Delta\rho}{\rho} \approx \frac{\Delta n_{\text{sup}}}{n_{\text{vol}}} \cdot \frac{1}{\text{thickness}}$$

where Δn_{sup} is the moved charge per unit area and n_{vol} is the total charge per unit volume. This is a linear relationship that crosses the axes origin. We then adjust the layer thickness t_{dl} in such a way that the effective thickness $t_{\text{eff}}=(t-t_{dl})$, that is film thickness t minus dead layer thickness t_{dl}, makes the plot of Fig. 12 intercept the axes origin. We find $t_{dl} \approx 2.7$ unit cells for the data points at $T=10$ K and $t_{dl} \approx 2$ unit cells for the data points at the resistivity minima. Moreover, from the slopes of Fig. 12, we obtain the effective charge density n_{eff} in the conducting atomic layers: we find $n_{\text{eff}} \approx 1.8 \cdot 10^{18}$ cm^{-3} at $T=10$ K and $n_{\text{eff}} \approx 2.5 \cdot 10^{18}$ cm^{-3} at the resistivity minima. In other words, we can think of the films as having nearly vanishing charge carriers in the t_{dl}–thick layers and then a nearly constant charge-carrier concentration n_{eff} in the remaining t_{eff}–thick layers. Obviously, the actual situation is certainly more gradual, but this estimate gives a useful rough indication. The value of $t_{dl} \approx 2$ unit cells, possibly divided into one unit cell at both $SrTiO_3$ interfaces, confirms that the charge depletion at the interface is a consequence of a short-range effect involving one or two atomic layers. Indeed, such a short range is expected from orbital redistribution by broken translational symmetry. On the other hand, the n_{eff} values are much smaller than the nominal charge concentration of $La_{0.7}Sr_{0.3}MnO_3$, $\sim 10^{21}$ cm^{-3}; we think that in these ultrathin films this effective value reflects the presence of semiconducting depleted regions at all temperatures down to 10 K, in the phase-separation picture confirmed by the nonvanishing colossal MR in the whole temperature range. These carrier-concentration values, on the other hand, are consistent with results extracted from the normal contribution to Hall effect.

In the bottom panel of Fig. 12, we plot the T_{MI} of the three samples A, B, and C at zero, positive, and negative applied gate voltages. The overall T_{MI} shift of sample C is the largest possible that can be obtained in our side-gate geometry, as the 6 unit cells and thinner samples are semiconducting at all temperatures and for all gate voltages.

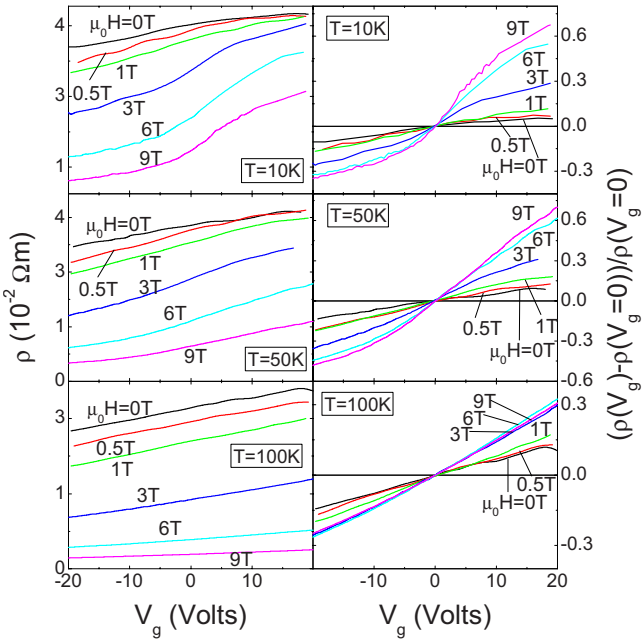

FIG. 13. (Color online) Left-hand panels: resistivity versus gate voltage curves of a 10 unit cells thick sample affected by strong localization effects (sample E) at different magnetic fields and temperatures. Right-hand panels: relative resistivity change. The magnetic field enhances rather than suppressing field effect.

C. Magnetotransport and field effect in disordered samples

The above described findings are similarly observed in all the metallic ultrathin samples. We now consider how localization effects change the effectiveness of combined electric and magnetic fields, with respect to the cleaner samples. Sample E is a 10 unit cells sample, where the localizing effects of disorder and/or enhanced strain due to slightly altered stoichiometry are responsible for lack of metallic behavior in the whole temperature range. In Fig. 13, the resistivity curves as a function of the gate voltage at different temperatures and magnetic fields present a striking difference with respect to the previous samples, namely that the largest field-effect modulation at any fixed temperature is obtained in a magnetic field $\mu_0 H=9$ T and the smallest is obtained in zero field, in a monotonic trend. On the other hand, in weakly disordered samples there is almost no dependence of field-effect modulation on magnetic field, which is just the crossing point behavior between the opposite trends of the samples free from disorder effects and the heavily disordered samples. The peculiar field-effect enhancement by a magnetic field has been already noticed in samples with transport across metallic regions below the percolation threshold,[25] and has been attributed to the fact that the magnetic field brings semiconducting regions closer to the transition point, making the electric field more effective in tuning their conductivity. This explanation holds in a phase-separation scenario, since in a homogeneous system, which is driven toward a more metallic state by the magnetic field, the opposite behavior should take place. However, beside this interpretation, we cannot rule out that the magnetic field may cause a modification in the band structure: for

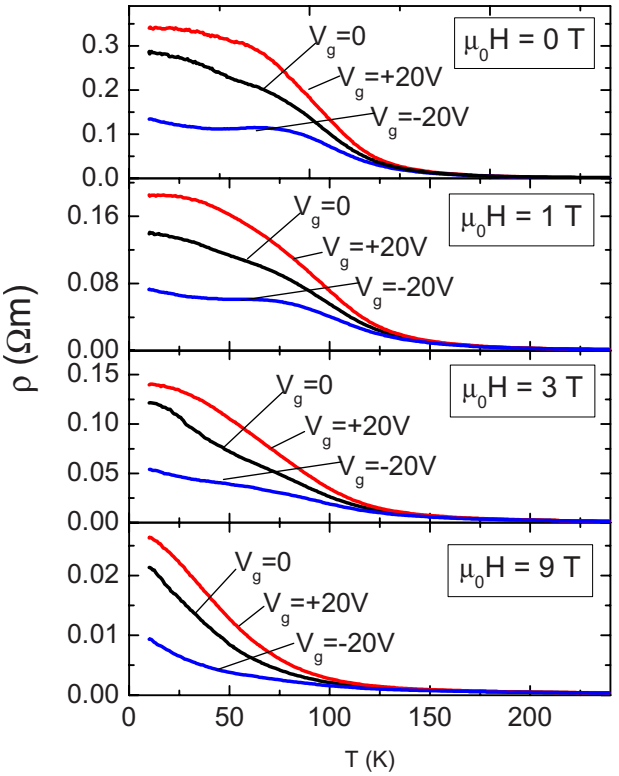

FIG. 14. (Color online) Resistivity versus temperature curves of the 10 unit cells thick disordered sample E at different magnetic fields and gate voltages.

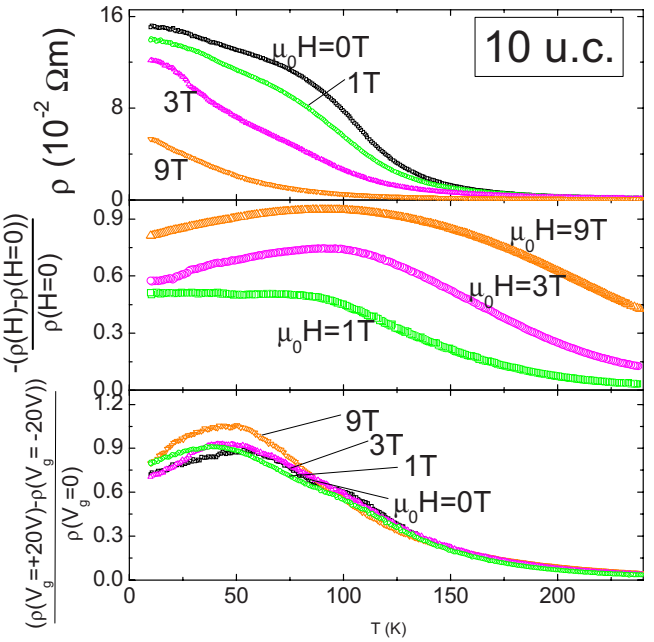

FIG. 15. (Color online) Top panel: resistivity versus temperature curves of the 10 unit cells thick disordered sample E at different magnetic fields. Middle panel: absolute value of negative magnetoresistivity as a function of temperature at different magnetic fields. Bottom panel: relative resistivity modulation by field effect as a function of temperature at different magnetic fields.

example, we can argue that the magnetic field increases the transfer integral of charge carriers, widens the bandwidth, and, for conservation of the total number of electronic states in the band, decreases the density of states. Thereby, in a system with lower density of states, the number of carriers at the Fermi level is smaller and the field-effect modulation is indeed expected to be larger. In Fig. 14, we show resistivity of sample E as a function of temperature at different fields and gate voltages. It can be noticed that the resistivity values are larger by two orders of magnitude than those measured for sample B having the same thickness. Field effect modulation reaches values similar to sample B, indicating that the semiconducting behavior is due to the localizing effect of disorder or strain, but not to severely lowered carrier density related to oxygen deficiency. Figure 15 evidences that the MR broad peak extends over the whole range of measured temperatures (middle panel), indicating a significant phase inhomogeneity in this sample. We also notice that, above 100 K, the field effect $[\rho(V_g=+20\ \mathrm{V})-\rho(V_g=-20\ \mathrm{V})]/\rho(V_g=0)$ (bottom panel) is weakly sensitive to the application of a magnetic field, a peculiar feature observed in many samples where localization effects are present. We also point out that this highly resistive sample exhibits nonlinear current-voltage characteristics at low temperature and even slight hysteresis, so that the curves of resistivity modulation as a function of temperature reported in the bottom panel of Fig. 15 are not the exact counterpart of the curves of resistivity modulation as a function of gate voltage reported in Fig. 13.

In summary, when localization mechanisms related with a random distribution of structural defects or strain are present, field effect is either almost independent (weak strain or disorder) or even enhanced (strong strain or disorder) by the magnetic field. Just the opposite occurs in case the spatial inhomogeneity is of electronic nature: the field effect is suppressed by the magnetic field in the phase-separation regime of samples not appreciably affected by structural disorder. In this respect, we remark the differences between 10–12 unit cells samples exhibiting localization by disorder or strain (sample E in this work) and 6 unit cells or thinner samples where localization occurs by some effect related to the proximity of the interface (sample D in this work): only in the latter sample field effect and MR are severely suppressed. These results point out the peculiarity of the localization mechanism active in the dead layer.

IV. CONCLUSIONS

Ultrathin $La_{0.7}Sr_{0.3}MnO_3$ films are ideal systems to study how band filling affects magnetotransport mechanisms and phase separation in this compound.

Our field-effect experiments indicate that magnetoresistivity and field effect induced resistivity modulation as a function of temperature exhibit similar broad peaks, a possible signature of the phase separated regime. The combined effects of electric and magnetic fields may sum up or balance, depending on the level of disorder in the sample.

We find that our films have a 6 unit cells thick dead layer, which is highly resistive and insensitive to band filling by field effect. On the contrary, in a 7 unit cells thick sample, we evidence the possibility of shifting the T_{MI} by as much as

43 K and tuning the resistivity up to 250% by a gate voltage. We rule out epitaxial strain, electronic reconstruction, and simple depletion of charge carriers by rigid-band shift at the interface to explain the behavior of the interface dead layer. Alternatively, on the basis of a model recently proposed by Tebano *et al.*,[51] we argue that proximity to interface and/or surface may be responsible for orbital redistribution, with suppression of double-exchange mechanism and consequent carrier localization. Such carriers localization applies as well to extra charges injected at the interface thus suppressing the field effect on the electrical conductivity in the dead layer.

ACKNOWLEDGMENTS

G.B. and A.T. thank Elettronica Masel s.r.l., for partial financial support of this work. I.P., L.P., E.B., A.S.S., and D.M. acknowledge support from the EU under the project Nanoxide, Contract No. 033191

[1] M. Bowen, M. Bibes, A. Barthélémy, J. P. Contour, A. Anane, Y. Lemaître, and A. Fert, Appl. Phys. Lett. **82**, 233 (2003).
[2] T. Wu, M. A. Zurbuchen, S. Saha, R.-V. Wang, S. K. Streiffer, and J. F. Mitchell, Phys. Rev. B **73**, 134416 (2006).
[3] M. P. Singh, W. Prellier, Ch. Simon, and B. Raveau, Appl. Phys. Lett. **87**, 022505 (2005).
[4] M. K. Lee, T. K. Nath, C. B. Eom, M. C. Smoak, and F. Tsui, Appl. Phys. Lett. **77**, 3547 (2000).
[5] Y. Lu, J. Klein, C. Höfener, B. Wiedenhorst, J. B. Philipp, F. Herbstritt, A. Marx, L. Alff, and R. Gross, Phys. Rev. B **62**, 15806 (2000).
[6] J. M. De Teresa, A. Barthélémy, A. Fert, J. P. Contour, F. Montaigne, and P. Seneor, Science **286**, 507 (1999).
[7] Moon-Ho. Jo, N. D. Mathur, and M. G. Bramire, Appl. Phys. Lett. **80**, 2722 (2002).
[8] I. Pallecchi, L. Pellegrino, A. Caviglia, E. Bellingeri, G. Canu, G. C. Gazzadi, A. S. Siri, and D. Marré, Phys. Rev. B **74**, 014434 (2006).
[9] J. Z. Sun, J. Magn. Magn. Mater. **202**, 157 (1999).
[10] S. Q. Liu, N. J. Wu, and A. Ignatiev, Appl. Phys. Lett. **76**, 2749 (2000).
[11] A. Baikalov, Y. Q. Wang, B. Shen, B. Lorenz, S. Tsui, Y. Y. Sun, Y. Y. Xue, and C. W. Chu, Appl. Phys. Lett. **83**, 957 (2003).
[12] Y. Yanagisawa, H. Tanaka, T. Kawai, and L. Pellegrino, Appl. Phys. Lett. **89**, 253121 (2006); H. J. Liu and C. K. Ong, Phys. Rev. B **74**, 052409 (2006).
[13] H. Tanaka, J. Zhang, and T. Kawai, Phys. Rev. Lett. **88**, 027204 (2001).
[14] N. Nakagawa, M. Asai, Y. Mukunoki, T. Susaki, and H. Y. Hwang, Appl. Phys. Lett. **86**, 082504 (2005).
[15] C. Mitra, P. Raychaudhuri, G. Köbernik, K. Dörr, K. H. Müller, L. Schultz, and R. Pinto, Appl. Phys. Lett. **79**, 2408 (2001).
[16] H. Katsu, H. Tanaka, and T. Kawai, Appl. Phys. Lett. **76**, 3245 (2000).
[17] H. Tanaka and T. Kawai, J. Appl. Phys. **88**, 1559 (2000).
[18] T. Zhao, S. B. Ogale, S. R. Shinde, R. Ramesh, R. Droopad, J. Yu, K. Eisenbeiser, and J. Misewich, Appl. Phys. Lett. **84**, 750 (2004).
[19] I. Pallecchi, L. Pellegrino, E. Bellingeri, A. S. Siri, and D. Marré, Appl. Phys. Lett. **83**, 4435 (2003).
[20] T. Kanki, Y. G. Park, H. Tanaka, and T. Kawai, Appl. Phys. Lett. **83**, 4860 (2003).
[21] X. Hong, A. Posadas, A. Lin, and C. H. Ahn, Phys. Rev. B **68**, 134415 (2003).
[22] F. X. Hu and J. Gao, Appl. Phys. Lett. **88**, 132502 (2006).
[23] M. Eblen-Zayas, A. Bhattacharya, N. E. Staley, A. L. Kobrinskii, and A. M. Goldman, Phys. Rev. Lett. **94**, 037204 (2005).
[24] T. Zhao, S. B. Ogale, S. R. Shinde, R. Ramesh, R. Droopad, J. Yu, K. Eisenbeiser, and J. Misevich, Appl. Phys. Lett. **84**, 750 (2004).
[25] I. Pallecchi, L. Pellegrino, E. Bellingeri, A. S. Siri, and D. Marré, Phys. Rev. B **71**, 014406 (2005).
[26] X. Hong, A. Posadas, and C. H. Ahn, Appl. Phys. Lett. **86**, 142501 (2005).
[27] T. Kanki, H. Tanaka, and T. Kawai, Appl. Phys. Lett. **89**, 242506 (2006).
[28] C. Thiele, K. Dörr, L. Schultz, E. Beyreuther, and W.-M. Lin, Appl. Phys. Lett. **87**, 162512 (2005).
[29] R. K. Zheng, Y. Wang, H. L. W. Chan, C. L. Choy, and H. S. Luo, Appl. Phys. Lett. **90**, 152904 (2007).
[30] X. Hong, J. B. Yau, J. D. Hoffman, C. H. Ahn, Y. Bason, and L. Klein, Phys. Rev. B **74**, 174406 (2006).
[31] T. Arnal, R. Soulimane, A. Aassime, M. Bibes, Ph. Lecoeur, A. M. Haghiri-Gosnet, B. Mercey, A. V. Khvalkovskii, A. K. Zvezdin, and K. A. Zvezdin, Microelectron. Eng. **78-79**, 201 (2005).
[32] L. Pellegrino, E. Bellingeri, A. S. Siri, and D. Marré, Appl. Phys. Lett. **87**, 064102 (2005).
[33] I. Pallecchi, L. Pellegrino, E. Bellingeri, A. S. Siri, and D. Marré, J. Appl. Phys. **95**, 8079 (2004).
[34] I. Pallecchi, L. Pellegrino, A. Caviglia, E. Bellingeri, G. Canu, G. C. Gazzadi, A. S. Siri, and D. Marré, Phys. Rev. B **74**, 014434 (2006).
[35] M. Angeloni, G. Balestrino, N. G. Boggio, P. G. Medaglia, P. Orgiani, and A. Tebano, J. Appl. Phys. **96**, 6387 (2004).
[36] S. Yunoki, A. Moreo, E. Dagotto, S. Okamoto, S. S. Kancharla, and A. Fujimori, Phys. Rev. B **76**, 064532 (2007).
[37] J. H. Park, E. Vescovo, H. J. Kim, C. Kwon, R. Ramesh, and T. Venkatesan, Phys. Rev. Lett. **81**, 1953 (1998).
[38] A. Ohtomo, D. A. Muller, J. L. Grazul, and H. Y. Hwang, Nature (London) **419**, 378 (2002); A. Ohtomo and H. Y. Hwang, *ibid.* **427**, 423 (2004).
[39] M. Nakamura, A. Sawa, H. Sato, H. Akoh, M. Kawasaki, and Y. Tokura, Phys. Rev. B **75**, 155103 (2007).
[40] S. Thiel, G. Hammerl, A. Schmehl, C. W. Schneider, and J. Mannhart, Science **313**, 1942 (2006).
[41] A. Ohtomo and H. Y. Hwang, Nature (London) **427**, 423 (2004).
[42] P. Kameli, H. Salamati, and A. Aezami, J. Appl. Phys. **100**, 053914 (2006).
[43] S. Roy, I. Dubenko, D. D. Edorth, and N. Ali, J. Appl. Phys. **96**, 1202 (2004).
[44] K. H. Ahn, T. Lookman, and A. R. Bishop, Nature (London) **428**, 401 (2004).

[45] J. Z. Sun, D. W. Abraham, R. A. Rao, and C. B. Eom, Appl. Phys. Lett. **74**, 3017 (1999).
[46] M. Bibes and S. Valencia, Ll. Balcells, B. Martínez, J. Fontcuberta, M. Wojcik, S. Nadolski, and E. Jedryka, Phys. Rev. B **66**, 134416 (2002).
[47] G. Herranz, M. Berkowski, E. Jedryka, M. Wojcik, F. Sánchez, M. Bibes, and J. Fontcuberta, J. Appl. Phys. **93**, 8065 (2003).
[48] R. P. Borges, W. Guichard, J. G. Lunney, J. M. D. Coey, and F. Ott, J. Appl. Phys. **89**, 3868 (2001).
[49] S. B. Ogale, Y. H. Li, M. Rajeswari, L. Salamanca Riba, R. Ramesh, T. Venkatesan, A. J. Millis, R. Kumar, G. K. Mehta, R. Bathe, and S. I. Patil, J. Appl. Phys. **87**, 4210 (2000).
[50] Y. Konishi, Z. Fong, M. Izumi, T. Manato, M. Kasai, H. Kuwahara, M. Kawasaki, K. Terakura, and Y. Tokura, J. Phys. Soc. Jpn. **68**, 3790 (1999).
[51] A. Tebano, C. Aruta, S. Sanna, P. G. Medaglia, G. Balestrino, A. A. Sidorenko, R. De Renzi, G. Ghiringhelli, L. Braicovich, V. Bisogni, and N. B. Brookes, Phys. Rev. Lett. **100**, 137401 (2008).
[52] H. Zenia, G. A. Gehring, G. Banach, and W. M. Temmerman, Phys. Rev. B **71**, 024416 (2005).
[53] A. Tebano, G. Balestrino, N. G. Boggio, C. Aruta, B. Davidson, and P. G. Medaglia, Eur. Phys. J. B **51**, 337 (2006).
[54] Software package TICOMP 5.0 by FieldPrecision, New Mexico, USA.
[55] H. M. Christen, J. Mannhart, E. J. Williams, and Ch. Gerber, Phys. Rev. B **49**, 12095 (1994).
[56] C. H. Ahn, J. M. Triscone, and J. Mannhart, Nature (London) **424**, 1015 (2003).
[57] N. Furukawa, J. Phys. Soc. Jpn. **66**, 2523 (1997).
[58] D. Wu, Z. H. Xiong, X. G. Li, Z. V. Vardeny, and J. Shi, Phys. Rev. Lett. **95**, 016802 (2005).
[59] Y. Lyanda-Geller, S. H. Chun, M. B. Salamon, P. M. Goldbart, P. D. Han, Y. Tomioka, A. Asamitsu, and Y. Tokura, Phys. Rev. B **63**, 184426 (2001).
[60] C. Aruta, G. Ghiringhelli, A. Tebano, N. G. Boggio, N. B. Brookes, P. G. Medaglia, and G. Balestrino, Phys. Rev. B **73**, 235121 (2006).